

OSCAR-based Reconstruction for Compressed Sensing and Parallel MR Imaging

L. El Gueddari ^{1,2}, P. Ciuciu ^{1,2}, E. Chouzenoux ^{3,4}, A. Vignaud ¹ and J.-C. Pesquet ³

¹CEA/NeuroSpin, Gif-sur-Yvette, France ²INRIA-CEA Saclay Ile-de-France, Parietal team, Univ Paris-Saclay, France ³CVN, Centrale-Supélec, Univ. Paris-Saclay, France ⁴LIGM, Paris-Est University, France

ISMRM 2019, Montreal, CAN



Outline

- 1 Motivation & Context
 - Why non-Cartesian acquisition
 - Non-Cartesian MR image reconstruction in parallel imaging
- 2 Calibration-less MR image reconstruction
 - Problem statement
 - Joint sparsity regularization
- 3 Experiments & Results
 - Experimental set-up
 - Results
- 4 Conclusion & Outlook

Anatomical MRI

Anatomical MRI is generally acquired using Cartesian sampling.

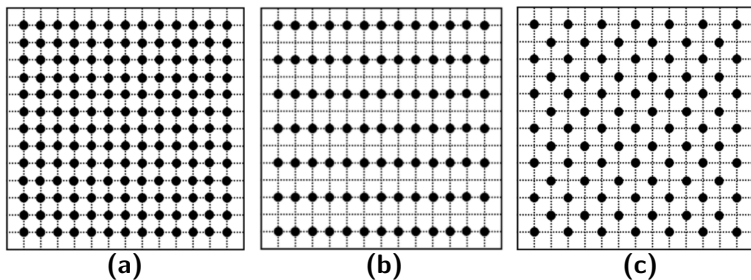


Figure: Typical (a) Cartesian (b) parallel acquisition (c) CAIPIRINHA¹ acquisition

... however in some cases non-Cartesian trajectories are useful ...

¹Breuer et al. 2006, *Magnetic Resonance in Medicine*.

Non-Cartesian trajectories for anatomical MRI

A non-exhaustive list of usages

- For ultra-short echo time imaging²
- X-nuclei imaging (TPI³)
- To correct for motion, especially for abdominopelvic MRI⁴

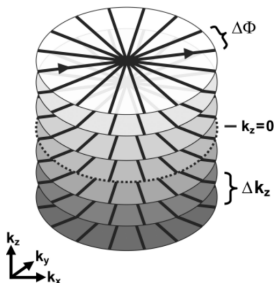


Figure: Stack of stars used for VIBE acquisition

²Johnson et al. 2013, *Magnetic Resonance in Medicine*.

³Boada et al. 1997, *Magnetic Resonance in Medicine*.

⁴Chandarana et al. 2014, *European radiology*.

Non-Cartesian trajectories for anatomical MRI

A non-exhaustive list of usages

- For ultra-short echo time imaging²
- X-nuclei imaging (TPI³)
- To correct for motion, especially for abdominopelvic MRI⁴

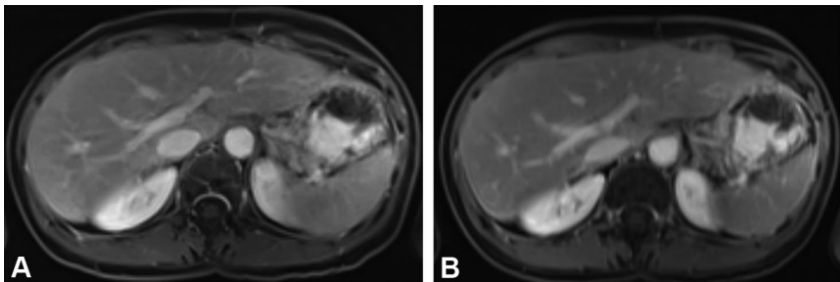


Figure: A: Free-breathing stack-of-stars VIBE, B: Breath-holding conventional VIBE

²Johnson et al. 2013, *Magnetic Resonance in Medicine*.

³Boada et al. 1997, *Magnetic Resonance in Medicine*.

⁴Chandarana et al. 2014, *European radiology*.

Non-Cartesian trajectories for anatomical MRI

Renewed interest to speed-up acquisition in the context of Compressed Sensing⁵.

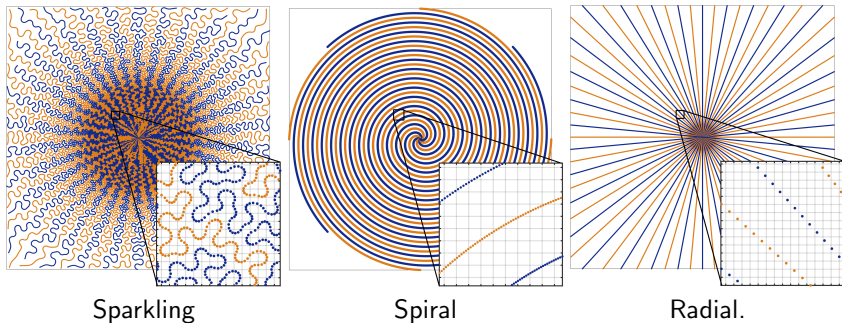


Figure: Example of non-Cartesian trajectories.

⁵Lazarus et al. 2019, *Magnetic Resonance in Medicine*.

Non-Cartesian trajectories for anatomical MRI

Renewed interest to speed-up acquisition in the context of Compressed Sensing⁵.

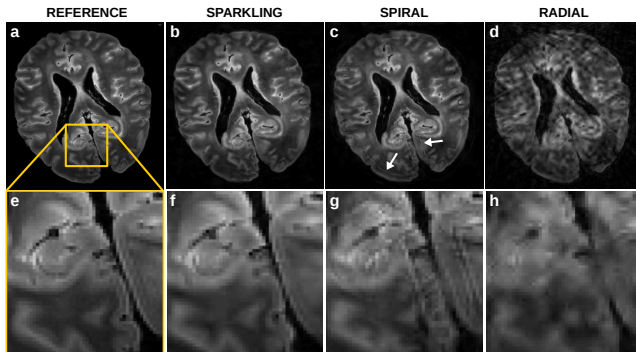


Figure: Comparison of different acquisition trajectories with 16-fold accelerated acquisition on T2*-weighted images.

⁵Lazarus et al. 2019, *Magnetic Resonance in Medicine*.

Non-Cartesian trajectories for anatomical MRI

Parallel imaging acquisition: collect multiple k-space data using a multi-receiver coil as the latter is known to boost the SNR.

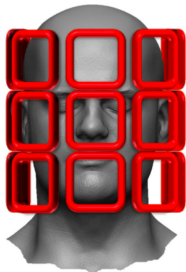


Illustration of multi-receiver coil (phased array).

Roemer et al. 1990, *Magnetic Resonance in Medicine*.

How do we reconstruct MR images from non-Cartesian k-space measurements in parallel imaging?

Non-Cartesian MR image reconstruction in parallel imaging

Self-calibrating methods

Non-Cartesian reconstruction techniques can be split in two categories:

- 1 Self-calibrating methods:

⁷Samsonov et al. 2004, *Magnetic Resonance in Medicine*.

⁸Uecker et al. 2014, *Magnetic Resonance in Medicine*.

Non-Cartesian MR image reconstruction in parallel imaging

Self-calibrating methods

Non-Cartesian reconstruction techniques can be split in two categories:

① Self-calibrating methods:

- require a region where the signal has been sampled at least at the Nyquist rate

⁷Samsonov et al. 2004, *Magnetic Resonance in Medicine*.

⁸Uecker et al. 2014, *Magnetic Resonance in Medicine*.

Non-Cartesian MR image reconstruction in parallel imaging

Self-calibrating methods

Non-Cartesian reconstruction techniques can be split in two categories:

1 Self-calibrating methods:

- require a region where the signal has been sampled at least at the Nyquist rate
- model the coil sensitivity profiles S_ℓ for all channels $\ell = 1, \dots, L$ ^{7,8}

⁷Samsonov et al. 2004, *Magnetic Resonance in Medicine*.

⁸Uecker et al. 2014, *Magnetic Resonance in Medicine*.

Non-Cartesian MR image reconstruction in parallel imaging

Self-calibrating methods

Non-Cartesian reconstruction techniques can be split in two categories:

1 Self-calibrating methods:

- require a region where the signal has been sampled at least at the Nyquist rate
- model the coil sensitivity profiles S_ℓ for all channels $\ell = 1, \dots, L$ ^{7,8}
- solve an inverse problem and recover a single full FOV image:

$$\hat{\mathbf{x}} = \arg \min_{\mathbf{x} \in \mathbb{C}^N} \frac{1}{2} \sum_{\ell=1}^L \sigma_\ell^{-2} \|F_\Omega S_\ell \mathbf{x} - \mathbf{y}_\ell\|_2^2 + \lambda \|\Psi \mathbf{x}\|_1 \quad (1)$$

- $\mathbf{y}_\ell \in \mathbb{C}^M$ the ℓ^{th} channel-specific data set
- $\mathbf{x} \in \mathbb{C}^N$ the reconstructed image (ex. $N = 512 \times 512$)
- F_Ω is the forward under-sampling Fourier operator
- $\Psi \in \mathbb{C}^{N_\Psi \times N}$ linear operator related to a sparse decomposition

⁷Samsonov et al. 2004, *Magnetic Resonance in Medicine*.

⁸Uecker et al. 2014, *Magnetic Resonance in Medicine*.

Non-Cartesian MR image reconstruction in parallel imaging

Self-calibrating methods

Non-Cartesian reconstruction techniques can be split in two categories:

1 Self-calibrating methods:

- require a region where the signal has been sampled at least at the Nyquist rate
- model the coil sensitivity profiles S_ℓ for all channels $\ell = 1, \dots, L$ ^{7,8}
- solve an inverse problem and recover a single full FOV image:

$$\hat{\mathbf{x}} = \arg \min_{\mathbf{x} \in \mathbb{C}^N} \frac{1}{2} \sum_{\ell=1}^L \sigma_\ell^{-2} \|F_\Omega S_\ell \mathbf{x} - \mathbf{y}_\ell\|_2^2 + \lambda \|\Psi \mathbf{x}\|_1 \quad (1)$$

- $\mathbf{y}_\ell \in \mathbb{C}^M$ the ℓ^{th} channel-specific data set
- $\mathbf{x} \in \mathbb{C}^N$ the reconstructed image (ex. $N = 512 \times 512$)
- F_Ω is the forward under-sampling Fourier operator
- $\Psi \in \mathbb{C}^{N_\Psi \times N}$ linear operator related to a sparse decomposition

Note: Extraction of coil sensitivity maps is challenging in non-Cartesian case

⁷Samsonov et al. 2004, *Magnetic Resonance in Medicine*.

⁸Uecker et al. 2014, *Magnetic Resonance in Medicine*.

Non-Cartesian MR Image reconstruction from multi-channel array coil acquisition

Calibration-less methods

Non-Cartesian reconstruction techniques can be split in two categories:

- 2 Calibration-less methods:
 - do not require any calibration region

⁹Trzasko and Manduca 2011, *Signals, Systems and Computers (ASILOMAR), 2011 Conference Record of the Forty Fifth Asilomar Conference on*.

¹⁰Majumdar and Ward 2012, *Magnetic Resonance in Medicine*.

Non-Cartesian MR Image reconstruction from multi-channel array coil acquisition

Calibration-less methods

Non-Cartesian reconstruction techniques can be split in two categories:

- 2 Calibration-less methods:
 - do not require any calibration region
 - solve an inverse problem but recover channel-specific images

⁹Trzasko and Manduca 2011, *Signals, Systems and Computers (ASILOMAR), 2011 Conference Record of the Forty Fifth Asilomar Conference on*.

¹⁰Majumdar and Ward 2012, *Magnetic Resonance in Medicine*.

Non-Cartesian MR Image reconstruction from multi-channel array coil acquisition

Calibration-less methods

Non-Cartesian reconstruction techniques can be split in two categories:

2 Calibration-less methods:

- do not require any calibration region
- solve an inverse problem but recover channel-specific images
- use the redundant information given by each coil to impose constraints such as low-rank CLEAR⁹ or group-sparsity CALM¹⁰

⁹Trzasko and Manduca 2011, *Signals, Systems and Computers (ASILOMAR), 2011 Conference Record of the Forty Fifth Asilomar Conference on*.

¹⁰Majumdar and Ward 2012, *Magnetic Resonance in Medicine*.

Non-Cartesian MR Image reconstruction from multi-channel array coil acquisition

Calibration-less methods

Non-Cartesian reconstruction techniques can be split in two categories:

2 Calibration-less methods:

- do not require any calibration region
- solve an inverse problem but recover channel-specific images
- use the redundant information given by each coil to impose constraints such as low-rank CLEAR⁹ or group-sparsity CALM¹⁰
- more likely to be used for on-line image reconstruction

⁹Trzasko and Manduca 2011, *Signals, Systems and Computers (ASILOMAR), 2011 Conference Record of the Forty Fifth Asilomar Conference on*.

¹⁰Majumdar and Ward 2012, *Magnetic Resonance in Medicine*.

Problem statement

Calibration-less MR image reconstruction problem solved using an *analysis formulation*:

Definition

MR image reconstruction is formulated as follows:

$$\hat{\underline{\mathbf{x}}} = \arg \min_{\underline{\mathbf{x}} \in \mathbb{C}^{N \times L}} \left\{ \frac{1}{2} \sum_{\ell=1}^L \sigma_{\ell}^{-2} \|F_{\Omega} \mathbf{x}_{\ell} - \mathbf{y}_{\ell}\|_2^2 + g(\mathbf{T} \underline{\mathbf{x}}) \right\}, \quad (2)$$

with:

- $\mathbf{y}_{\ell} \in \mathbb{C}^M$ the ℓ^{th} channel-specific data set
- $\mathbf{x}_{\ell} \in \mathbb{C}^N$ the ℓ^{th} channel-specific reconstructed image (ex. $N = 512 \times 512$)
- F_{Ω} is the forward under-sampling Fourier operator
- $\mathbf{T} \in \mathbb{C}^{N_{\psi} \times N}$ linear operator related to a sparse decomposition
- g is a convex regularization term that promotes sparsity

Optimization algorithm

Primal dual optimization

We aim to find:

$$\hat{\underline{\mathbf{x}}} \in \underset{\underline{\mathbf{x}} \in \mathbb{C}^{N \times L}}{\operatorname{argmin}} [f(\underline{\mathbf{x}}) + g(\mathbf{T}\underline{\mathbf{x}})] \quad (3)$$

where:

- f is convex, differentiable on $\mathbb{C}^{N \times L}$ and its gradient is β -Lipschitz
- $g \in \Gamma_0(\mathbb{C}^{N_\Psi \times L})$ ¹¹ with a closed form proximity operator, given by:

$$\operatorname{prox}_g(\underline{\mathbf{z}}) = \underset{\underline{\mathbf{v}} \in \mathbb{C}^{N_\Psi \times L}}{\operatorname{argmin}} \frac{1}{2} \|\underline{\mathbf{z}} - \underline{\mathbf{v}}\|^2 + g(\underline{\mathbf{v}}) \quad (4)$$

Note: Those are standard assumptions in optimization based image reconstruction methods.

¹¹ Γ_0 is the set of convex proper lower semi-continuous functions on $\mathbb{C}^{N_\Psi \times L}$ taking values on $\mathbb{R} \cup \inf$

Optimization algorithm

Condat-Vũ sequence

Using a primal-dual optimization method proposed by Condat-Vũ^{12,13}:

Algorithm 1: Condat-Vũ algorithm

initialize $k = 0$, $\tau > 0$, $\kappa > 0$, $\underline{\mathbf{x}}_0$, $\underline{\mathbf{z}}_0$;

while $k \leq K$ **do**

$$\underline{\mathbf{x}}_{k+1} := \underline{\mathbf{x}}_k - \tau (\nabla f(\underline{\mathbf{x}}_k) + \mathbf{T}^* \underline{\mathbf{z}}_k);$$

$$\underline{\mathbf{w}}_{k+1} := \underline{\mathbf{z}}_k + \kappa \mathbf{T} (2\underline{\mathbf{x}}_{k+1} - \underline{\mathbf{x}}_k);$$

$$\underline{\mathbf{z}}_{k+1} := \underline{\mathbf{w}}_{k+1} - \kappa \operatorname{prox}_{g/\kappa} \left(\frac{\underline{\mathbf{w}}_{k+1}}{\kappa} \right);$$

end

with:

- the algorithm weakly converges to the solution of Eq. (3) if

$$\frac{1}{\tau} - \kappa \|\mathbf{T}\|^2 \geq \frac{\beta}{2}$$

- τ and κ hyper-parameters set as follows: $\tau := \frac{1}{\beta}$, $\kappa := \frac{\beta}{2\|\mathbf{T}\|^2}$

¹²Condat 2013, *Journal of Optimization Theory and Applications*.

¹³Vũ 2013, *Advances in Computational Mathematics*.

Joint sparsity regularization

Group-LASSO

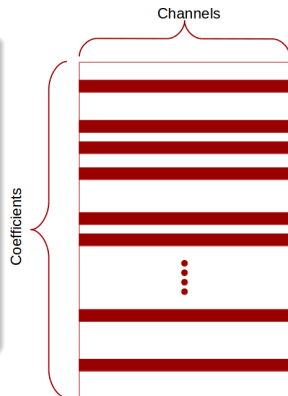
Parallel imaging has been proved to have tighter recovery guarantees than single channel acquisition when combined with Group-LASSO (GL) regularization¹⁴.

Definition

The group-LASSO penalty is defined as follows:

$$g_{GL}(\underline{z}) = \|\underline{z}\|_{1,2} = \sum_{s=1}^S \left(\lambda \gamma^s \sum_{p=1}^{P_s} \sqrt{\sum_{\ell=1}^L |z_{spl}|^2} \right)$$

- λ and γ are positive hyper-parameters
- s models the scale or subband dependence



¹⁴Chun, Adcock, and Talavage 2016, *IEEE Transactions on Medical Imaging*.

For $\gamma = 1$ the algorithm corresponds to Majumdar and Ward, *Magnetic Resonance in Medicine*, 2012

Joint sparsity regularization

Sparse group-LASSO

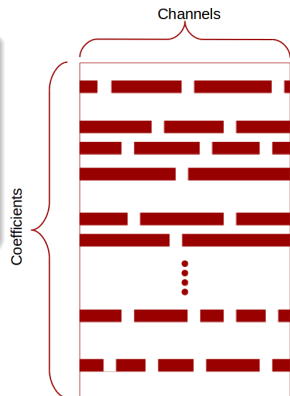
Variant: Sparse group-LASSO¹⁶ (sGL)

Definition

$$\forall \underline{z} \in \mathbb{C}^{N_\psi \times L}, g_{\text{sGL}}(\underline{z}) = g_{\text{GL}}(\underline{z}) + \mu \|\underline{z}\|_1 \quad (5)$$

- μ being positive hyper-parameter.

sGL proximity operator¹⁸ is closed form and corresponds to the composition of GL proximity operator with soft-thresholding.



¹⁶Friedman, Hastie, and Tibshirani 2010, *arXiv preprint arXiv:1001.0736*.

Joint sparsity regularization

Octagonal Shrinkage and Clustering Algorithm for Regression

Inferring the structure via a pairwise l_∞ norm.

OSCAR regularization¹⁷ is defined as follows:

Definition

$$\begin{aligned} g_{\text{OSCAR}}(\mathbf{z}) &= \sum_{s=1}^S \lambda \left[\sum_{j=1}^{P_s L} |z_{sj}| + \gamma \sum_{j < k} \max\{|z_{sj}|, |z_{sk}|\} \right] \\ &= \sum_{s=1}^S \lambda \left[\sum_{j=1}^{P_s L} (\gamma(j-1) + 1) |z_{sj}|_{\downarrow} \right] \end{aligned} \quad (6)$$

where:

- $\underline{z}_{\downarrow} \in \mathbb{C}^{N_{\psi} \times L}$ the wavelet coefficients sorted in decreasing order, i.e.: $\forall s \in \mathbb{N}, |z_{s1}| \leq \dots \leq |z_{sP_s L}|$.
- λ and γ are some positive hyper-parameters that need to be set

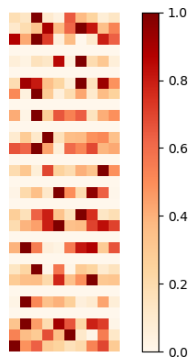


Figure: Original wavelet coefficients (WC)

¹⁷Bondell and Reich 2008, *Biometrics*.

Joint sparsity regularization

Octagonal Shrinkage and Clustering Algorithm for Regression

Inferring the structure via a pairwise ℓ_∞ norm.

OSCAR regularization¹⁷ is defined as follows:

Definition

$$\begin{aligned} g^{\text{OSCAR}}(\mathbf{z}) &= \sum_{s=1}^S \lambda \left[\sum_{j=1}^{P_s L} |z_{sj}| + \gamma \sum_{j < k} \max\{|z_{sj}|, |z_{sk}|\} \right] \\ &= \sum_{s=1}^S \lambda \left[\sum_{j=1}^{P_s L} (\gamma(j-1) + 1) |z_{sj}|_{\downarrow} \right] \quad (6) \end{aligned}$$

where:

- $\mathbf{z}_{\downarrow} \in \mathbb{C}^{N_{\psi} \times L}$ the wavelet coefficients sorted in decreasing order, i.e.: $\forall s \in \mathbb{N}, |z_{s1}| \leq \dots \leq |z_{sP_s L}|$.
- λ and γ are some positive hyper-parameters that need to be set

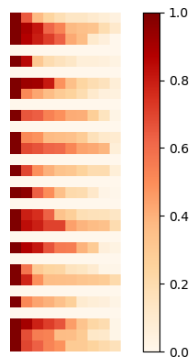


Figure: Sorted out WC in descending magnitude order



¹⁷Bondell and Reich 2008, *Biometrics*.

Joint sparsity regularization

Octagonal Shrinkage and Clustering Algorithm for Regression

Inferring the structure via a pairwise l_∞ norm.

OSCAR regularization¹⁷ is defined as follows:

Definition

$$\begin{aligned} g_{\text{OSCAR}}(\mathbf{z}) &= \sum_{s=1}^S \lambda \left[\sum_{j=1}^{P_s L} |z_{sj}| + \gamma \sum_{j < k} \max\{|z_{sj}|, |z_{sk}|\} \right] \\ &= \sum_{s=1}^S \lambda \left[\sum_{j=1}^{P_s L} (\gamma(j-1) + 1) |z_{sj}|_{\downarrow} \right] \quad (6) \end{aligned}$$

where:

- $\underline{z}_{\downarrow} \in \mathbb{C}^{N_{\psi} \times L}$ the wavelet coefficients sorted in decreasing order, i.e.: $\forall s \in \mathbb{N}, |z_{s1}| \leq \dots \leq |z_{sP_s L}|$.
- λ and γ are some positive hyper-parameters that need to be set

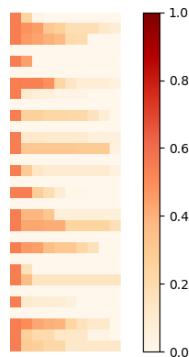


Figure: Thresholded sorted WC

¹⁷Bondell and Reich 2008, *Biometrics*.

Joint sparsity regularization

Octagonal Shrinkage and Clustering Algorithm for Regression

Inferring the structure via a pairwise l_∞ norm.

OSCAR regularization¹⁷ is defined as follows:

Definition

$$\begin{aligned} g_{\text{OSCAR}}(\mathbf{z}) &= \sum_{s=1}^S \lambda \left[\sum_{j=1}^{P_s L} |z_{sj}| + \gamma \sum_{j < k} \max\{|z_{sj}|, |z_{sk}|\} \right] \\ &= \sum_{s=1}^S \lambda \left[\sum_{j=1}^{P_s L} (\gamma(j-1) + 1) |z_{sj}|_{\downarrow} \right] \end{aligned} \quad (6)$$

where:

- $\underline{z}_{\downarrow} \in \mathbb{C}^{N_{\psi} \times L}$ the wavelet coefficients sorted in decreasing order, i.e.: $\forall s \in \mathbb{N}, |z_{s1}| \leq \dots \leq |z_{sP_s L}|$.
- λ and γ are some positive hyper-parameters that need to be set

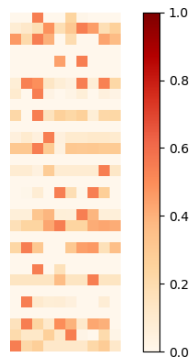


Figure: Unsorting WC to their original position

¹⁷Bondell and Reich 2008, *Biometrics*.

Experimental set-up

Sequence parameters:

- Ex-vivo baboon brain
- 7T Siemens Scanner GRE
- 1Tx/32Rx Nova coil
- Sparkling trajectory
- $390\mu\text{m} \times 390\mu\text{m}$ in plane-resolution
- 3mm slice thickness
- Acceleration factor of 15 in time
- Under-sampling factor of 2.5
- T : Undecimated Bi-Orthogonal 7-9 wavelet transform

Hyper-parameters set using a grid-search procedure.

Cartesian scan 512×512 was acquired and used for reference.

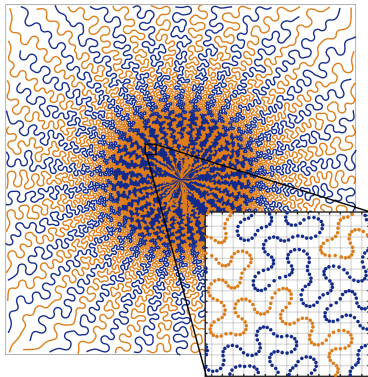


Figure: Sparkling trajectory

Results

Quantitative assessment

Coil combination: Square root of the Sum-Of-Squares
Structural SIMilarity Index (SSIM)¹⁸ used to set hyper-parameters

Table: Image quality assessment for all regularizers.

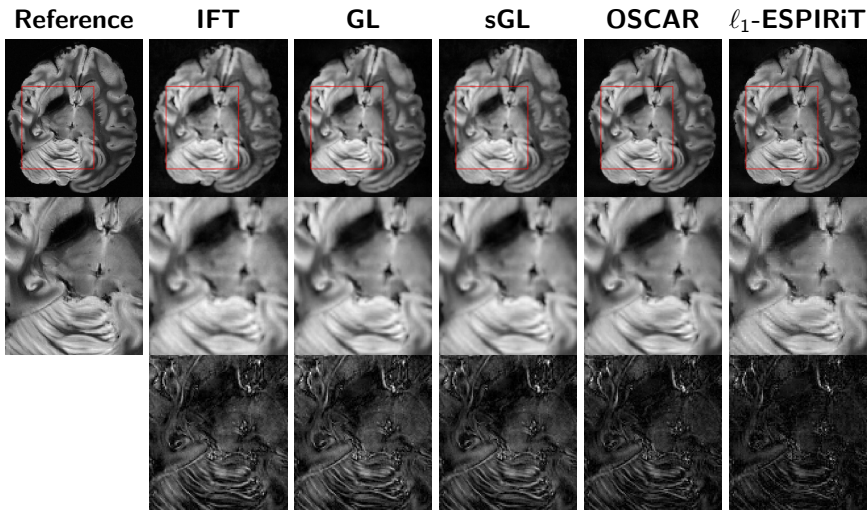
	SSIM	pSNR (dB)	NRMSE
IFT	0.847	26.50	0.263
GL	0.864	26.92	0.254
sGL	0.851	26.77	0.259
OSCAR	0.875	30.49	0.177
ℓ_1 -ESPIRiT	0.874	28.32	0.238

Note: ℓ_1 -ESPIRiT is a self-calibrating method.

¹⁸Wang et al. 2004, *IEEE transactions on image processing*.

Results

Comparison of the Sum-Of-Squares



Results

Quantitative assessment

Comparison between coil images:

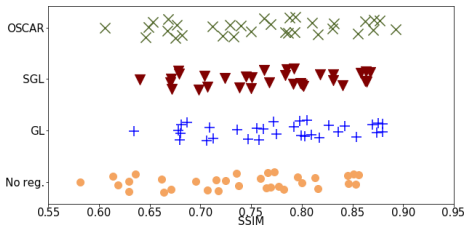


Figure: Assessment of the SSIM score per channel.

Results

Quantitative assessment

Comparison between coil images:

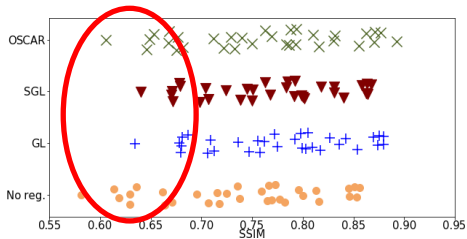
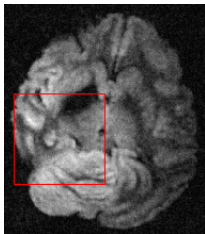


Figure: Assessment of the SSIM score per channel.

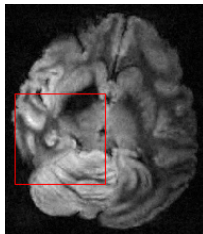
Results

Comparison of the image channels: low-SNR channel

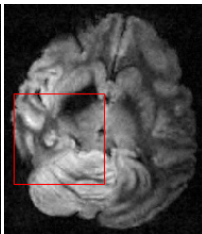
No reg.
SSIM= 0.630



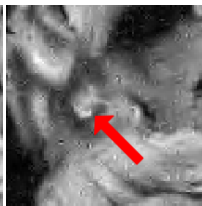
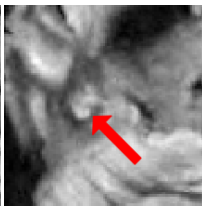
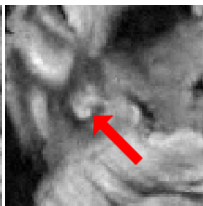
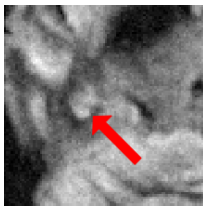
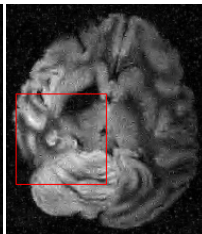
Group-LASSO
SSIM= 0.680



Sparse GL
SSIM= 0.672



OSCAR
SSIM= 0.646



Results

Quantitative assessment

Comparison between coil images:

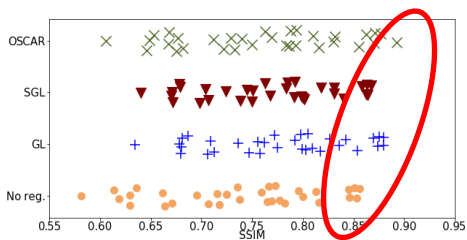


Figure: Assessment of the SSIM score per channel.

Results

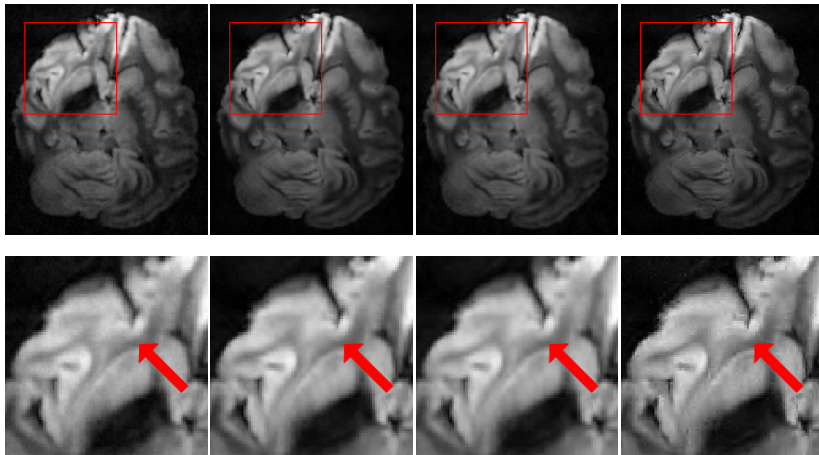
Comparison of the image channels: high-SNR channel

No reg.
SSIM= 0.846

Group-LASSO
SSIM= 0.880

Sparse GL
SSIM= 0.863

OSCAR
SSIM= 0.893



Conclusion & Outlook

Conclusion:

- New parallel CS-MRI reconstruction algorithm
- No sensitivity maps
- OSCAR outperforms group-LASSO and sparse group-LASSO
- OSCAR and ℓ_1 -ESPIRiT are comparable, however the latest is self-calibrating
- Same optimization method to solve calibration-less MR reconstruction

Perspectives:

- Extension to 3D-MRI
- Study motion impact on the reconstruction

Code is available on : [LElgueddari/pysap/calibrationless_p_mri_reconstruction](https://github.com/LElgueddari/pysap/calibrationless_p_mri_reconstruction)



Acknowledgement

This project have been granted by the mobility grant of the SFRMBM and the FLI society



References I

- Boada, Fernando E. et al. (1997). “Fast three dimensional sodium imaging”. In: *Magnetic Resonance in Medicine* 37.5, pp. 706–715.
- Bondell, H.D. and B.J. Reich (2008). “Simultaneous regression shrinkage, variable selection, and supervised clustering of predictors with OSCAR”. In: *Biometrics* 64.1, pp. 115–123.
- Breuer, Felix A et al. (2006). “Controlled aliasing in volumetric parallel imaging (2D CAIPIRINHA)”. In: *Magnetic Resonance in Medicine* 55.3, pp. 549–556.
- Chandarana, Hersh et al. (2014). “Free-breathing contrast-enhanced T1-weighted gradient-echo imaging with radial k-space sampling for paediatric abdominopelvic MRI”. In: *European radiology* 24.2, pp. 320–326.
- Chun, I.Y., B. Adcock, and T.M. Talavage (2016). “Efficient compressed sensing SENSE pMRI reconstruction with joint sparsity promotion”. In: *IEEE Transactions on Medical Imaging* 35.1, pp. 354–368.
- Condat, L. (2013). “A primal–dual splitting method for convex optimization involving Lipschitzian, proximable and linear composite terms”. In: *Journal of Optimization Theory and Applications* 158.2, pp. 460–479.

References II

- Friedman, J., T. Hastie, and R. Tibshirani (2010). “A note on the group lasso and a sparse group lasso”. In: *arXiv preprint arXiv:1001.0736*.
- Johnson, Kevin M. et al. (2013). “Optimized 3D ultrashort echo time pulmonary MRI”. In: *Magnetic Resonance in Medicine* 70.5, pp. 1241–1250.
- Lazarus, Carole et al. (2019). “SPARKLING: variable-density k-space filling curves for accelerated T2*-weighted MRI”. In: *Magnetic Resonance in Medicine* 81.6, pp. 3643–3661.
- Majumdar, A.I and R.K. Ward (2012). “Calibration-less multi-coil MR image reconstruction”. In: *Magnetic Resonance in Medicine* 30.7, pp. 1032–1045.
- Roemer, P.B. et al. (1990). “The NMR phased array”. In: *Magnetic Resonance in Medicine* 16.2, pp. 192–225.
- Samsonov, Alexei A et al. (2004). “POCSSENSE: POCS-based reconstruction for sensitivity encoded magnetic resonance imaging”. In: *Magnetic Resonance in Medicine* 52.6, pp. 1397–1406.
- Trzasko, J.D. and A. Manduca (2011). “Calibrationless parallel MRI using CLEAR”. In: *IEEE*, pp. 75–79.

References III

- Uecker, M. et al. (2014). “ESPIRiT– an eigenvalue approach to autocalibrating parallel MRI: where SENSE meets GRAPPA”. In: *Magnetic Resonance in Medicine* 71.3, pp. 990–1001.
- Vũ, BC (2013). “A splitting algorithm for dual monotone inclusions involving cocoercive operators”. In: *Advances in Computational Mathematics* 38.3, pp. 667–681.
- Wang, Zhou et al. (2004). “Image quality assessment: from error visibility to structural similarity”. In: *IEEE transactions on image processing* 13.4, pp. 600–612.